Corrosion Science, Vol. 32, No. 1, pp. 37–50, 1991
Printed in Great Britain

0010–938X/91 $3.00 + 0.00
Pergamon Press plc

IRON DISSOLUTION AND PASSIVATION IN K_2CO_3–$KHCO_3$ SOLUTIONS. ROTATING RING DISC ELECTRODE AND XPS STUDIES

E. B. CASTRO, J. R. VILCHE and A. J. ARVIA

Instituto de Investigaciones Fisicoquimicas Teóricas y Aplicadas (INIFTA), Facultad de Ciencias Exactas, Universidad Nacional de La Plata, Sucursal 4, C.C. 16, (1900), La Plata, Argentina

Abstract—Rotating ring-disc electrode studies on the anodic dissolution and passivation of iron in potassium carbonate/bicarbonate buffers at 25°C show that in the active anodic dissolution potential range Fe(II) soluble species are generated. This reaction is favoured by the presence of bicarbonate ions in solution and it is explained through the formation of an unstable soluble complex containing Fe(II) and HCO_3^- ions. This suggests that the anodic layer at a certain stage of its formation contains some amount of carbonate species. XPS data of surface layers produced at different anodic potentials confirm the presence of the carbonate species in thick anodic layers grown in the prepassive potential region in still solutions, whereas the opposite result is found for the thin passive layers formed at high positive potentials.

INTRODUCTION

THE corrosion and passivation of Fe in alkaline aqueous solutions as well as the active to passive transition and vice versa, depend on the solution composition.[1–4] These processes in alkaline media occur through the initial formation of an oxygen-containing surface species usually assigned to $Fe(OH)_{ad}$,[4–6] and the onset of passivity initiates with the formation of a $Fe(OH)_2$ layer which subsequently grows to form a composite layer.[7–11] This passive layer can be described as an inner Fe_3O_4 layer and an outer hydrous FeOOH which becomes a matrix where the Fe(III)/Fe(II) redox reactions can be observed.[12,13] This description is derived from *in-situ* Raman spectroscopy,[14–16] X-ray photo-electron spectroscopy after specimen preparation and transfer into an oxygen-free closed system,[17] Mössbauer spectroscopy,[18,19] and ellipsometry.[20–22] The validity of this interpretation covers a very wide range of pH for solutions where either aggressive anions are absent or anions which form poorly soluble iron salts are present, as is the case for Fe in carbonate–bicarbonate containing solutions.

Previous works[23–26] on the electrodissolution and passivation of polycrystalline Fe electrodes in potassium carbonate/bicarbonate buffers based upon electrochemical measurements, concluded that the interaction between Fe^{2+} and HCO_3^- ions plays an important role, particularly at the outer part of the prepassive layer where the local pH becomes determined by the appropriate anodic reaction coupled to different Fe ionic species equilibria. According to this interpretation soluble Fe^{2+} and Fe^{3+} species should be formed in the course of the anodic and cathodic processes involving the direct participation of CO_3^{2-}/HCO_3^- ions.

The purpose of the present work is to demonstrate the formation of soluble species during the anodisation of Fe in K_2CO_3–$KHCO_3$ solutions through the use of

Manuscript received 15 November 1989.

the rotating ring disc electrode technique and to provide information about the composition of the passivating surface layer through XPS analysis.[27–29]

EXPERIMENTAL METHOD

The experimental arrangement was the same as described elsewhere.[23,24] The formation of soluble iron species during the voltammetric sweep of Fe electrodes immersed in carbonate–bicarbonate-containing solutions was followed through a rotating ring-disc electrode (RRDE). The latter consisted of a polycrystalline Fe disc ('Specpure', Johnson Matthey Chemicals Ltd, 0.40 cm dia.) and a polycrystalline Au ring (0.44 and 0.50 cm inner and outer dia., respectively), with a collection efficiency, $N_T = 0.27$.[30] Before each electrochemical run, the electrode arrangement was successively polished with 400 and 600 grade emery papers and 1.0 and 0.3 μm grit alumina–acetone suspensions, and afterwards repeatedly rinsed with triply distilled water. Finally, the Fe electrode was polarised for 30 s at potentials sufficiently negative to produce hydrogen evolution. This treatment furnished a reproducible electroreduced Fe surface. The electrical circuitry was completed with a large area Pt plate counter electrode and a SCE reference electrode properly shielded and connected to the rest of the cell through a Luggin–Haber capillary tip, although potentials in the text are referred to the NHE scale.

The electrolyte solutions consisted of a mixture of x M $KHCO_3$ + y M K_2CO_3 ($0.075 \leq x \leq 2.5$; $0.0015 \leq y \leq 1.5$), covering the pH 8.4–10.5 range. At each pH, values of x and y were set to cover a wide ionic strength range by keeping the HCO_3^-/CO_3^{2-} concentration ratio constant. Solutions were prepared from analytical grade (Merck) reagents and triply distilled water previously boiled to remove CO_2. Experiments were made under purified N_2 gas saturation at 25°C.

Single triangular potential sweeps (STPS) were applied to the Fe electrode between preset cathodic ($E_{s,c}$) and anodic ($E_{s,a}$) switching potentials, at potential sweep rates (v) within the $0.001 \leq 0.100$ V s^{-1} range. The rotation speed (ω) of the RRDE was maintained at $\omega = 1000$ rpm.

X-Ray photo-electron spectroscopy (XPS) measurements were performed with an ESCA B-Mark II equipment. For this purpose, polycrystalline Fe electrodes in the form of discs (0.070 cm^2 apparent area) resulting from axially embedding an Fe rod in a PTFE tube and cutting the piece at a right angle in the lathe, were employed in quiescent solutions.

EXPERIMENTAL RESULTS AND INTERPRETATION

Rotating ring-disc electrode data

Voltammograms of Fe in 0.75 M $KHCO_3$ + 0.15 M H_2CO_3, pH 9.5, run at $\omega = 1000$ rpm and different scan rates between $E_{s,c} = -0.86$ V and $E_{s,a} = 0.24$ V, are shown in Fig. 1(a). Thus, at $v = 0.01$ V s^{-1} the voltammogram in the positive potential direction exhibits firstly the HER current, and then two anodic current contributions (I and II) at -0.64 and -0.42 V, respectively, and in the reverse direction a small cathodic current at *ca* -0.43 V followed by an anodic current peak (anodic reactivation) located at -0.53 V, and again the HER current at potentials more negative than -0.7 V. The situation changes in the voltammogram run at 0.1 V s^{-1}, since in this case an extended anodic current plateau is recorded during the positive potential going direction between -0.20 and 0.24 V. The corresponding reverse scan shows a broad although small cathodic current peak (IV) at *ca* -0.45 V instead of anodic reactivation. The identification of current peaks follows that used in previous publications.[23,24] In this case, when the Au ring electrode is held at $E_R = 0.74$ V (Fig. 1b), the formation of soluble Fe(II) species becomes evident in the potential range of peaks I, II and IV and also in the anodic reactivation region of the Fe disc electrode voltammogram. The maximum amount of soluble Fe(II) species appears very close to the potential of peak II. Conversely, no soluble Fe(II) species can be detected when the potential applied to the Fe disc is greater than -0.2 V (passivity region). Nevertheless, the experimental collection efficiencies derived at the potential of peak II from Fig. 1, $N_{exp} = 0.12$ for $v = 0.01$ V s^{-1} and $N_{exp} = 0.11$ for $v = 0.1$ V s^{-1}, are considerably smaller than the theoretical value,

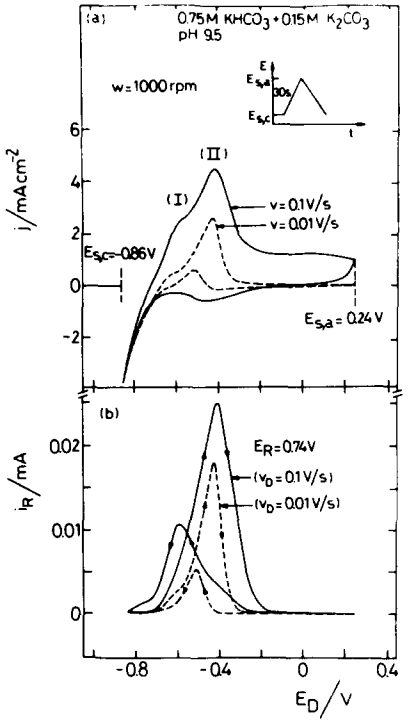

FIG. 1. RRDE current vs potential plots: 0.75 M $KHCO_3$ + 0.15 M K_2CO_3, pH 9.5, ω = 1000 rpm. (a) Fe disc electrode data; (b) Au ring electrode data, E_R = 0.74 V; v = 0.1 V s^{-1} (——) and v = 0.01 V s^{-1} (– – –); 25°C.

N_T = 0.27. This suggests that the faradaic processes occurring at the Fe disc involve the formation of both insoluble and soluble Fe(II) species.

The correlation between peak IV in the voltammogram of the Fe disc and the current hump at about the same potential observed in the negative potential direction I_R/E_D profile obtained at 0.1 V s^{-1}, suggests that the reduction of some constituent of the anodic layer produced in the positive potential going scan produces simultaneously soluble Fe(II) species. Such a process has been described for Fe passive layer electroreduction in buffer borate electrolyte.[8,10]

At a constant pH the heights of the voltammetric peaks I and II as well as the magnitude of the anodic reactivation, increase considerably with the HCO_3^- ion concentration. Correspondingly, an anodic current contribution appears at the Au ring (Fig. 2). Otherwise, for a constant HCO_3^- concentration within the 8.9 to 10.5 pH range, a change in the CO_3^{2-} ion concentration produces only a slight negative potential shift of the various current peak potentials on increasing pH (Fig. 3) on the entire electrochemical response of the RRDE. The influence of $E_{s,a}$ on the RRDE response was particularly considered at pH 10.5 (Fig. 4). It becomes clear that with increasing $E_{s,a}$, the anodic reactivation peak diminishes progressively, and finally it is replaced by the cathodic peak IV. Furthermore, the electroreduction of the anodic layer produced by sweeping the potential up to 1.04 V is accompanied by the appearance of a double anodic current peak at the ring. This fact can be associated with a sequence of electroreduction reactions yielding soluble Fe(II) directly.

In order to demonstrate the formation of soluble Fe(III) species during the anodisation of Fe, voltammetric runs were also made at the RRDE by keeping the Au ring at $E_R = -0.66$ V to indicate the soluble Fe(III) species through its electroreduction reaction to Fe(II) (Fig. 5). The corresponding results show that Fe(III) species are produced at the Fe disc when the applied potential is greater than -0.35 V. Under these conditions the currents at both the Fe disc and the Au ring reach limiting values. This behaviour suggests that on the passive layer either a diffusion control or a chemical dissolution reaction is determining the total anodic process at the Fe disc.

The interpretation of RRDE data

The RRDE data can provide information about the order of magnitude for the rate of formation of soluble Fe(II) and the Fe(II) concentration both at the electrode surface and in the bulk of the solution. It should be noticed that in the present case an exact evaluation of RRDE data becomes extremely difficult because the ionic transport at the interface involves a complex multicomponent system at a film covered electrode. However, this situation can be simplified by considering that the electrode behaves as a rotating flat disc involving only the Fe(II) species concentration profile extending from the reaction layer to the bulk of the solution. Correspondingly, the pH profile as well as the ionic equilibria involving Fe(II) species are neglected. It is further assumed that the process at the Fe disc occurs under quasi-steady conditions in the potential range of peak II ($j_{p,II}$). The latter can be justified because in the voltammograms at Fe disc electrodes run at a scan rate $v \leq 0.025$ V s^{-1}, $j_{p,II}$ becomes practically independent of v (Fig. 6). This simplified

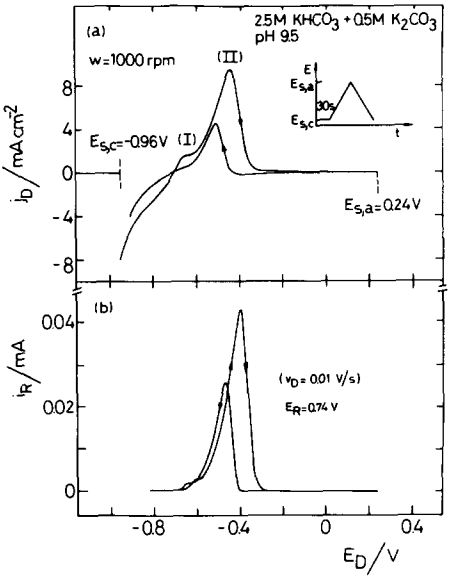

FIG. 2. RRDE current vs potential plots: 2.5 M $KHCO_3$ + 0.5 M K_2CO_3, pH 9.5, $\omega = 1000$ rpm. (a) Fe disc electrode data; (b) Au ring electrode data; $E_R = 0.74$ V, $v_D = 0.01$ V s^{-1}; 25°C.

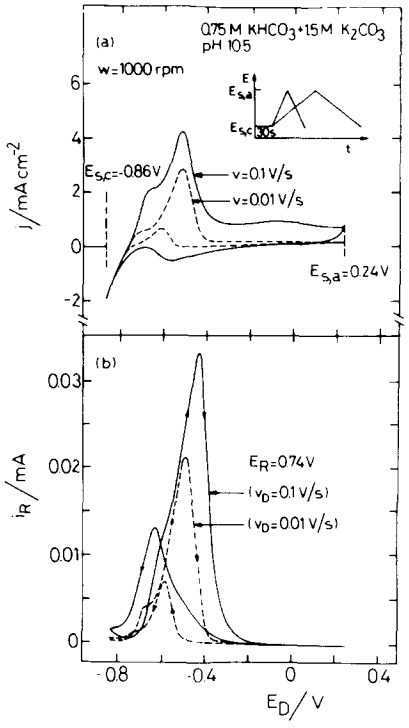

FIG. 3. RRDE current vs potential plots: 0.75 M $KHCO_3$ + 1.5 M K_2CO_3, pH 10.5, ω = 1000 rpm. (a) Fe disc electrode data; (b) Au ring electrode data; E_R = 0.74 V, v_D = 0.01 V s^{-1}; 25°C.

approach allows concentration data to be estimated and relevant qualitative information about the participation of anions in the process to be derived.

For this purpose the diffusion coefficient of Fe(II) species in the carbonate–bicarbonate solutions was determined by using a Au disc electrode (0.07 cm^2 apparent area) in 1.5 M $KHCO_3$ + z M $Fe(NH_4)_2(SO_4)_2.6H_2O$ solution ($0.0001 \leq z \leq 0.0014$). The anodic limiting current density, j_L, for the reaction Fe(II) = Fe(III) + e^- was measured in the 300 rpm $\leq w \leq$ 3000 rpm range. Figure 7 shows the linear j_L vs $w^{1/2}$ plots for different concentrations of the Fe(II) salt. The value of $D_{Fe(II)}$ was derived from the slope of the linear j_L vs $w^{1/2}$ relationship, by considering Levich's equation[31] with n, the number of electrons involved in the reaction at the disc equal to one, and $c^*_{Fe(II)}$, the corresponding concentration of the Fe(II) salt in solution. The resulting value at 25°C is $D_{Fe(II)} = 3 \times 10^{-6}$ cm^2 s^{-1}. This figure becomes practically independent of the Fe(II) salt concentration and is comparable to data reported in the literature for the Fe^{2+} ion in other solutions.

Let us now consider the current detected at the ring electrode, I_R, when $E_D = E_{p,II}$. If I_D is the total current at the disc electrode under a certain applied potential value, then $I_{D,c}$, the fraction of I_D related to Fe(II) soluble species, can be expressed in terms of I_R as follows.

$$I_{D,c} = [I_R(n_D/n_R)/N_T] = \alpha I_D \tag{1}$$

where $0 \leq \alpha \leq 1$ and $N_T = 0.27$, $n_D = 2$ is the number of electrons involved in the reaction at the Fe disc electrode:

$$Fe = Fe(II)(aq) + 2\,e^-, \tag{2}$$

and $n_R = 1$ is the number of electrons participating at the Au ring electrode reaction:

$$Fe(II)(aq) = Fe(III)(aq) + 1\,e^-. \tag{3}$$

Under stationary conditions:

$$I_{D,c} = 2F\bar{J}_{Fe(II)} \tag{4}$$

where $\bar{J}_{Fe(II)}$ is the flow of Fe(II) species from the Fe disc surface outwards. Hence, from the rate of transport of Fe(II), the dissolution current $I_{D,c}$ (A cm^{-2}) at the disc electrode can be expressed through Levich's equation:

$$I_{D,c} = -0.62\,2FAD_{Fe(II)}^{2/3}\,\nu^{-1/6}\,\Delta c\,\omega^{1/2} \tag{5}$$

where $D_{Fe(II)}$ (cm^2 s^{-1}) is the diffusion coefficient of soluble Fe(II) in carbonate–bicarbonate solutions, A (cm^2) is the disc electrode geometric area, $\Delta c = c^*_{Fe(II)} - c^s_{Fe(II)}$ is the difference between the FE(II) concentration (mole cm^{-3}) in the bulk of the solution and at the Fe disc electrode surface, respectively, ω (s^{-1}) is the rotation speed of the RRDE, ν (cm^2 s^{-1}) is the kinematic viscosity of the solution, and F (coulomb eq^{-1}) is Faraday's constant.

By using $D_{Fe(II)} = 3 \times 10^{-6}$ cm^2 s^{-1}, $\nu = 0.01$ cm^2 s^{-1}, $\omega = 1000$ rpm $= 104.7$ s^{-1}, $N_T = 0.27$, and $A = 0.126$ cm^2, one obtains from equations (1) and (5):

$$\Delta c = kI_R \tag{6}$$

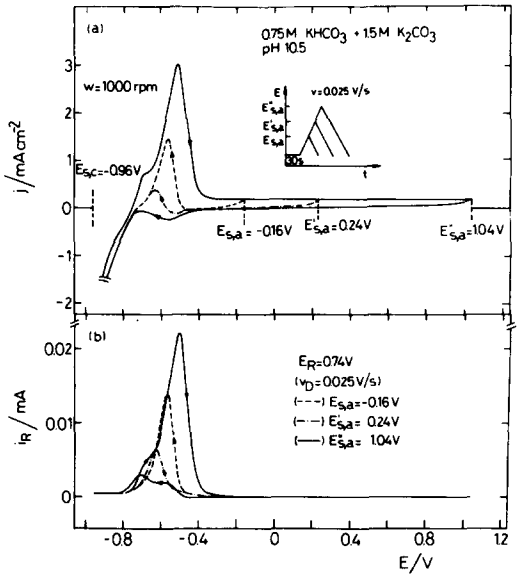

FIG. 4. The influence of $E_{s,a}$ on RRDE current vs potential plots. (a) Fe disc; (b) Au ring data at $v_D = 0.025$ V s^{-1} in 0.75 M $KHCO_3$ + 1.5 M K_2CO_3, pH 10.5, $\omega = 1000$ rpm, $E_R = 0.74$ V; 25°C.

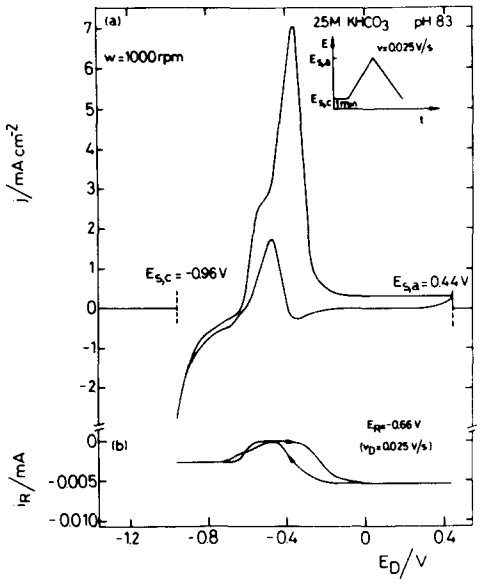

FIG. 5. RRDE current vs potential plots. (a) Fe disc data; (b) Au ring data, $E_R = 0.74$ V; 2.5 M $KHCO_3$ + 0.5 M K_2CO_3, pH 9.5, $v_D = 0.01$ V s^{-1}; $\omega = 1000$ rpm; 25°C.

where $k = 0.108$ eq A^{-1} cm^{-3}, I_R is given in A, so that Δc results in eq cm^{-3}. In order to estimate the value of $c^s_{Fe(II)}$, let us assume that $c^*_{Fe(II)} \ll \Delta c$, so that $\Delta c \approx c^s_{Fe(II)}$.

To justify this assumption, one can estimate $n_{Fe(II)}$, the total amount of soluble Fe(II) species produced at the disc electrode, by sweeping the potential from $E_{s,c} = -0.86$ V up to $E_{p,II}$, from the value of Q_R, the anodic charge detected at the Au ring for $E_R = 0.74$ V. This charge is related to $Q_{D,c}$, the charge involved in the generation of soluble Fe(II) at the Fe disc, through the expression:

$$Q_{D,c} = Q_R(n_D/n_R)/N_T. \tag{7}$$

Equation (7) allows to estimate the total number of moles of soluble Fe(II):

$$n_{Fe(II)} = Q_{D,c}/2F. \tag{8}$$

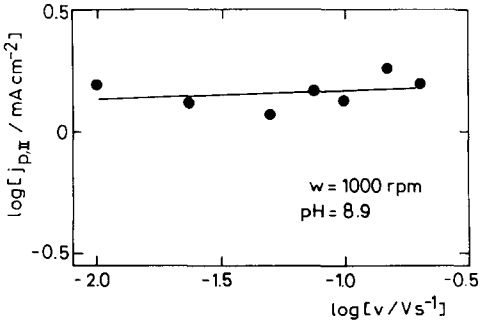

FIG. 6. The dependence of $j_{p,II}$ on v; 0.75 M $KHCO_3$ + 0.05 M K_2CO_3, pH 8.9; $\omega = 1000$ rpm; 25°C.

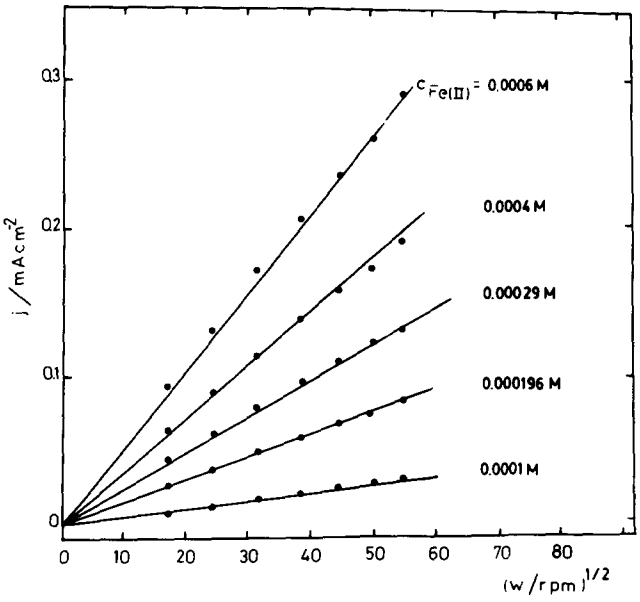

FIG. 7. The dependence of j_L on $w^{1/2}$. Au disc electrode; 1.5 M $KHCO_3$ + z M $Fe(NH_4)_2(SO)_4.6H_2O$ at different Fe(II) salt concentrations.

The values of $c^*_{Fe(II)}$ can be approximated to the average concentration $\langle c^*_{Fe(II)} \rangle$ derived from $n_{Fe(II)}$ and the electrochemical cell volume (*ca* 0.3 cm^3). Under the present working conditions the values of Δc fall between 10^{-3} and 10^{-4} mole dm^{-3}, and those of $\langle c^*_{Fe(II)} \rangle$ are in the 10^{-8}–10^{-9} mole dm^{-3} range. On the other hand, the concentration of Fe(II)(aq) calculated from the solubility products of either $Fe(OH)_2$ or $FeCO_3$ ($K_{sp}[Fe(OH)_2] = 8 \times 10^{-16}$ and $K_{sp}[FeCO_3] = 5.7 \times 10^{-11}$)[32,33] are close to the $c^*_{Fe(II)}$ values.

These results indicate that for the anodisation of Fe in K_2CO_3–$KHCO_3$ solutions the values of $c^s_{Fe(II)}$ exceed by far those predicted from solubility data of $Fe(OH)_2$ and $FeCO_3$. This difference can be explained to the fact that the Fe dissolution in these media is assisted by the presence of HCO_3^- ions. This is consistent with the linear $\log j_{D,c}$ vs $\log c_{HCO_3^-}$ plot obtained in the $8.9 \leq pH \leq 10.5$ range at $E = E_{p,II}$ (Fig. 8) whose slope is practically equal to unity, independently of pH and CO_3^{2-} ion concentration. Therefore, the RRDE data demonstrate the participation of HCO_3^- ion in the anodic dissolution of Fe through the formation of Fe(II) soluble species probably $[HCO_3Fe]^+$ or $Fe(CO_3H)_2$ complex ion species. From these results one can infer that the composite struture of the passivating layer under certain conditions involve the presence of carbonate-containing species. Direct information about this matter can be obtained from XPS data.

XPS data

The composition of the anodic layer formed on Fe in different conditions was determined by XPS to about 900 Å in depth. The following specimens were analysed. Specimen E_1 was polarised for 120 min at −0.43 V, that is at $E_{p,II}$, in still 0.75 M $KHCO_3$ + 0.05 M K_2CO_3 solution. Specimen E_2 was held at −0.18 V, i.e. in the passive potential region, in the same still solution for 120 min. Specimen E_3 was

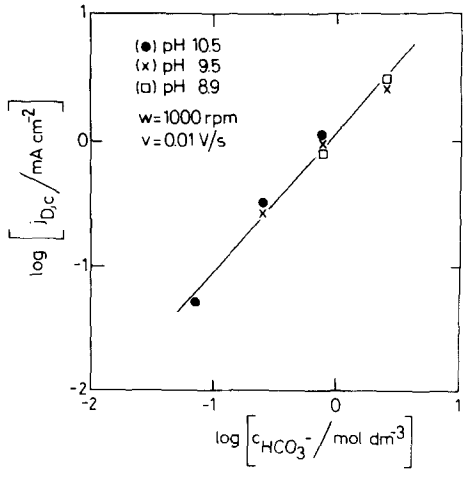

FIG. 8. Log $j_{D,c}(E_D = E_{p,II})$ vs log $c_{HCO_3^-}$ plot; $v = 0.01$ V s^{-1}; Carbonate–bicarbonate buffers covering different pH and ionic strength values; $\omega = 1000$ rpm; 25°C.

anodised in still 0.1 M NaOH for 120 min at potentials located in the net passivity range. Specimen E_4 was treated similarly to Specimen E_1 but previously subjected to ethanol cleaning, drying, and Au metallising to protect the surface film formed at $E_{p,II}$. To determine the presence of Fe, O, and C the XPS spectra (Figs 9 to 12) were obtained at different depths $0 \leq d \leq 900$ Å.[34,35]

The XPS results can be summarised as follows. Specimens E_2 and E_3 which were polarised in the passive region exhibit the Fe signal corresponding to Fe_2O_3 to a

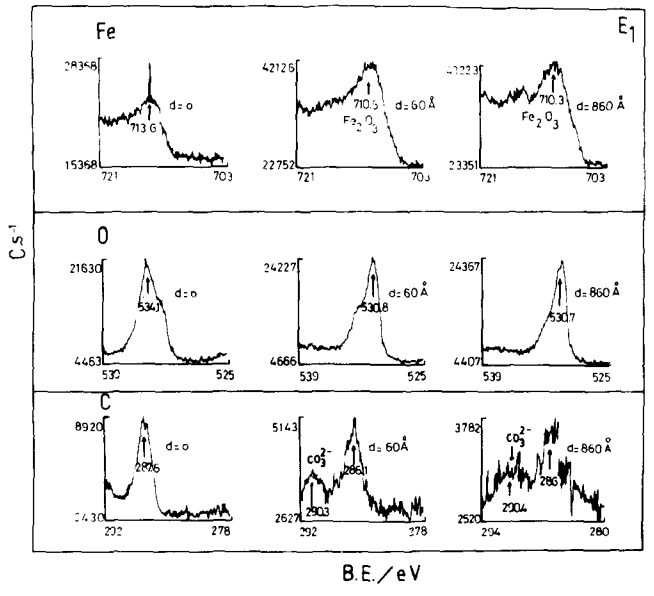

FIG. 9. XPS spectra obtained with an Fe disc electrode polarised in still 0.75 M $KHCO_3$ + 0.05 M K_2CO_3 for 120 min at $E_{p,II}$. The Fe, O and C peaks for different anodic layer depths are indicated.

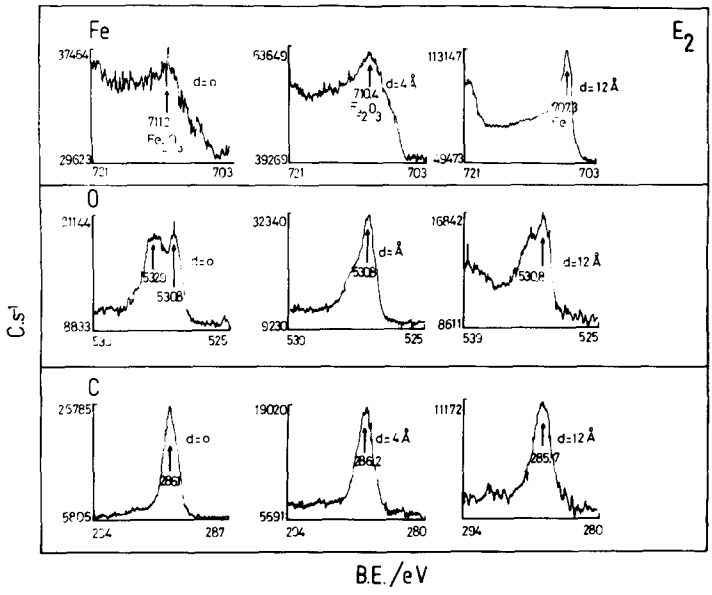

FIG. 10. XPS spectra corresponding to an Fe disc electrode polarised in still 0.75 M $KHCO_3$ + 0.05 M K_2CO_3 for 120 min in the passivity potential range.

depth of $d < 12$ Å (Figs 10 and 11). For $d > 12$ Å, the main peak at 707.3 eV corresponds exclusively to the Fe substrate. The intensity of O-atom signal follows that of the Fe peak in Fe_2O_3. As far as the C atom spectrum is concerned, the signal at *ca* 286 eV should be attributed to C-contamination which already existed in the

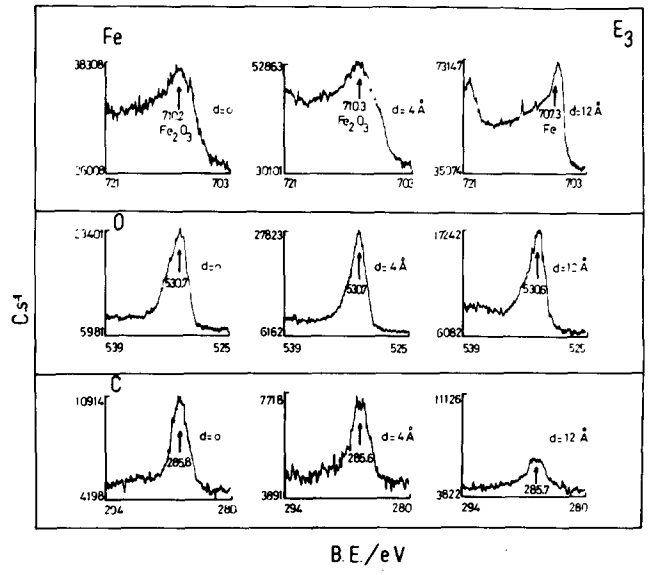

FIG. 11. XPS spectra corresponding to an Fe disc electrode polarised in 0.1 M NaOH for 120 min in the passivity potential range.

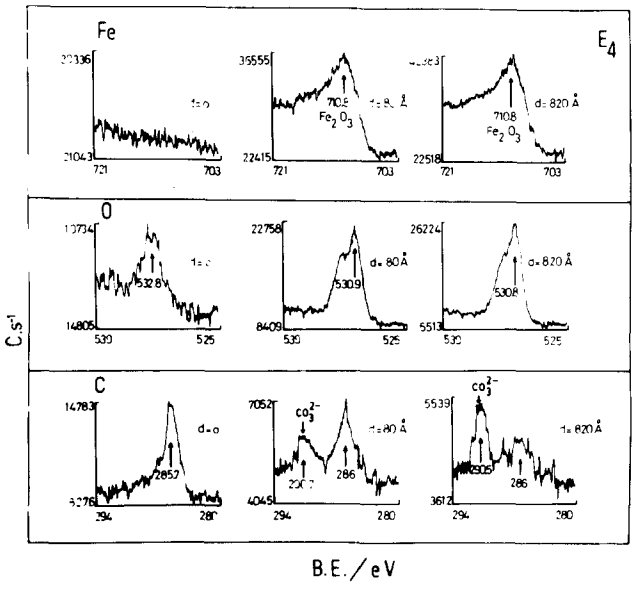

FIG. 12. XPS spectra corresponding to an Fe disc electrode polarised for 120 min at $E_{p,II}$ in still 0.75 M $KHCO_3$ + 0.05 M K_2CO_3 and subsequently Au metallised.

residual spectrometer atmosphere. Specimens E_1 and E_4 which were polarised at $E_{p,II}$, show the formation of thick anodic layers. In this case the appearance of Fe_2O_3 reaches a depth of about 860 Å (Figs 9 and 12) and the presence of CO_3^{2-}-species in the film can be concluded from the signal detected at 290.9 eV.

In conclusion, XPS data reveal the existence of carbonate containing species in the thick layers formed at low anodic polarisation in still solutions, whereas no C-signal (as CO_3^{2-}) could be detected in the thin passive layers produced at high positive potentials.

DISCUSSION

From previous studies[23–26] covering a wide range of v, ω, and ionic strengths, it becomes clear that the active to passive transition of Fe in carbonate–bicarbonate buffers involves at least two stages associated with the anodic peaks I and II. Peak I can be related to the surface formation of $Fe(OH)_2$ according to the overall reaction:

$$Fe + 2H_2O \rightleftharpoons Fe(OH)_2 + 2H^+ + 2e^- \quad (9)$$

although RRDE results clearly show (Figs 1–3) that reaction (9) occurs together with the dissolution of Fe producing also soluble Fe(II) species. The latter reaction becomes the major contribution in the potential range of peak II, including the anodic reactivation in the reverse negative potential going voltammetric scan. At potentials close to $E_{p,II}$ the gradual formation of Fe_3O_4 as a constituent of the passive layer takes place.[24]

For all electrolyte solutions used in this work, the RRDE results indicate that the concentration of soluble Fe(II) species at the Fe disc electrode largely exceeds the expected equilibrium concentration for either $Fe(H_2O)_6^{2+}$ or $Fe(OH)^+$ species under saturation conditions with $Fe(OH)_2$ and $FeCO_3$ as derived from the corresponding

K_{sp} values. Therefore, those large Fe(II) concentration values resulting from the anodic dissolution of Fe in carbonate–bicarbonate buffers must be associated with the formation of soluble compounds containing Fe(II) and HCO_3^-, probably $FeHCO_3^+$ and $Fe(HCO_3)_2$, instead of a local supersaturation of $Fe(OH)_2$ or $FeCO_3$. This conclusion emerges from the linear $\log j_{D,c}$ vs $\log c_{HCO_3^-}$ relationship with a slope close to one (Fig. 8). The possible formation of $Fe(CO_3)_2^{2-}$ has also been postulated,[36] but this type of complex has only been detected in solid state as part of the salt $K_2Fe(CO_3)_2 . 4H_2O$.

The formation of soluble Fe(II) species at relatively high positive potentials makes possible the appearance of insoluble compounds through a dissolution–precipitation mechanism. Accordingly, the local saturation of soluble Fe(II) species at the disc electrode/solution interface, particularly in the absence of forced convection, should favour the precipitation of $FeCO_3$ through a sequence of reactions such as:

$$FeHCO_3^+(aq) \rightleftharpoons Fe(II)(aq) + HCO_3^-(aq) \tag{10}$$

$$Fe(II)(aq) + CO_3^{2-}(aq) \rightleftharpoons FeCO_3(s). \tag{11}$$

The XPS results show that carbonate species appear in the composition of the anodic layers formed by polarising the Fe specimens in the potential range of peak II in quiescent carbonate–bicarbonate buffers solution (Figs 9 and 12). The corresponding anodic layer can then exceed 850 Å in thickness. The formation of such a thick type of anodic layers can be understood through the participation of a dissolution–precipitation process.

The $FeCO_3$-containing anodic layer precipitated on the Fe disc surface in quiescent solutions undergoes oxidation at more positive potentials.[24] Thus, the anodic process occurring in the potential range of peak III appears to be the same already reported for the same solutions in the absence of stirring at potentials close to that where the onset of passivity takes place.[24] The reaction related to peak III can be stated as follows:

$$2FeCO_3 + 3H_2O \rightleftharpoons \gamma\text{-}Fe_2O_3 + 2CO_3^{2-} + 6H^+ + 2\,e^-. \tag{12}$$

The equilibrium potential of reaction (12) at pH 8.9 and $c_{CO_3^{2-}} = 0.05$ M lies close to -0.172 V.[37] In contrast to previous descriptions, the XPS results obtained with Fe passivated electrodes (Figs 10 and 11) show very little differences between Fe specimens passivated either in carbonate–bicarbonate buffers or in NaOH solutions. In both cases the anodic layer thicknesses are smaller than 10 Å, Fe_2O_3 being the only constituent detected in the anodic layers.

According to RRDE results soluble Fe(II) species are also produced during the electroreduction of iron oxide formed at potentials more positive than 0 V (Fig. 4). This fact is in agreement with results reported in the literature about 15 years ago for the electroreduction of thin γ-FeOOH layers.[38] For this reaction no magnetite was detected as reaction product and the total cathodic charge was related to the formation of Fe(II) species. Correspondingly, the cathodic process occurs through the reduction of Fe(III) species with the simultaneous protonation of the oxide yielding a thin reduced Fe(II) containing layer which subsequently generates soluble Fe(II) species as follows:

$$\gamma\text{-FeOOH(s)} + H^+(aq) + e^- \rightleftharpoons \{Fe.OH.OH\}(s)(\text{thin reduced film}) \quad (13)$$

$$\{Fe.OH.OH\}(s) \rightleftharpoons Fe(II)(aq) + 2OH^-(aq). \quad (14)$$

The overall process represented by reactions (13) and (14) can favour the formation of $FeHCO_3^+$ which is determined by the equilibrium:

$$Fe(II)(aq) + HCO_3^-(aq) \rightleftharpoons FeHCO_3^+(aq). \quad (15)$$

The total or partial electroreduction of the passivating layers on Fe gives rise to a further contribution of soluble Fe(II) species[39,40] by releasing the Fe(II) species retained in the anodic layer, as the latter can be ascribed to a composite structure containing both Fe(III) and Fe(II) species.

The conclusions derived from the present work are in agreement with recent attempts to correlate ellipsometric and RRDE results in carbonate buffer at pH 9.2 which led to postulate that the iron passivation occurs initially through a dissolution–precipitation process yielding a ferrous hydroxide or basic ferrous carbonate layer, whereas in the passive range results are consistent with a thin inner mixed-valence layer and an outer hydrated layer essentially free of ferrous species at high anodic potential.[41]

Acknowledgements—This work was supported by the Consejo Nacional de Investigaciones Cientificas y Técnicas (Argentina) and the Comisión de Investigaciones Cientificas (Provincia de Buenos Aires).

REFERENCES

1. G. Nazri, E. Yeager and B. D. Cahan, Tech. Rep. No 1, Proj. NR SRO-005/7-30-79. Case Western Reserve University, Cleveland (1981).
2. K. E. Heusler, in *Encyclopedia of Electrochemistry of the Elements* (ed. A. J. Bard), Vol. 9A, pp. 229–381. Marcel Dekker, New York (1982).
3. S. Juanto, J. O. Zerbino, M. I. Miguez, J. R. Vilche and A. J. Arvia, *Electrochim. Acta* **32**, 1743 (1987).
4. W. J. Lorenz and K. E. Heusler, in *Corrosion Mechanisms* (ed. F. Mansfeld), p. 1. Marcel Dekker, New York (1987).
5. R. S. Schrebler Guzmán, J. R. Vilche and A. J. Arvia, *J. appl. Electrochem.* **11**, 551 (1981).
6. J. O. Zerbino, J. R. Vilche and A. J. Arvia, *J. appl. Electrochem.* **11**, 703 (1981).
7. V. Brusic, in *Oxides and Oxide Films* (ed. J. W. Diggle), pp. 1–89. Marcel Dekker, New York (1972).
8. N. Sato, in *Passivity of Metals* (ed. R. P. Frankenthal and J. Kruger), pp. 29–58. The Electrochemical Society Inc., Princeton (1978).
9. R. S. Schrebler Guzmán, J. R. Vilche and A. J. Arvia, *Electrochim Acta* **24**, 395 (1979).
10. N. Sato and G. Okamoto, in *Comprehensive Treatise of Eletrochemistry* (ed. J. O'M. Bockris, B. E. Conway, E. Yeager and R. E. White), Vol. 4, pp. 193–249. Plenum Press, New York (1981).
11. N. Brinda-Konopik, G. Nauer,H. Neugebauer and P. Schneyder, *DECHEMA-Monographic* **92**, 207 (1982)
12. V. A. Macagno, J. R. Vilche and A. J. Arvia, *J. appl. electrochem.* **11**, 417 (1981).
13. M. E. Vela, J. R. Vilche and A. J. Arvia, *Electrochim. Acta* **31**, 1633 (1986).
14. M. Froelicher, A. Hugot-Le Goff, C. Pallota, R. Dupeyrat and M. Mason, in *Passivity of Metals and Semiconductors* (ed. M. Froment), pp. 101–105. Elsevier, Amsterdam (1983).
15. J. Dünnwald and A. Otto, *Z. Anal. Chem.* **319**, 738 (1984).
16. J. C. Rubin and J. Dünnwald, *J. electroanal. Chem.* **258**, 327 (1989).
17. S. Haupt, C. Calinski, V. Collisi, H. W. Hoppe, H. D. Speckmann and H. H. Strehblow, *Surf. Interface Anal.* **9**, 357 (1986).
18. H. Kubsch, E. Fritzsch and H. A. Schneider, *Neve Hütte* **19**, 303 (1974).
19. C. Fierro, R. E. Carbonio, D. Scherson and E. B. Yeager, *J. Phys. Chem.* **91**, 6597 (1987).
20. Z. Q. Huang and J. L. Ord, *J. electrochem. Soc.* **132**, 24 (1985).

21. O. A. ALBANI, J. O. ZERBINO, J. R. VILCHE and A. J. ARVIA, *Electrochim. Acta* **31**, 1403 (1986).
22. S. JUANTO, J. O. ZERBINO, J. R. VILCHE and A. J. ARVIA, in *Surfaces, Inhibition, and Passivation* (eds E. MCCAFFERTY and R. J. BRODD), pp. 226–238. The Electrochemical Society Inc., Pennington (1986).
23. C. R. VALENTINI, C. A. MOINA, J. R. VILCHE and A. J. ARVIA, *Corros. Sci.* **25**, 985 (1985).
24. E. B. CASTRO, C. R. VALENTINI, C. A. MOINA, J. R. VILCHE and A. J. ARVIA, *Corros. Sci.* **26**, 781 (1986).
25. B. E. CASTRO, L. M. GASSA and J. R. VILCHE, *Proc. 10th Int. Congr. Met. Corros.*, pp. 2071–2079. Oxford & Ibh Publishing Co., New Delhi (1987).
26. R. H. MILOCCO, E. B. CASTRO, S. G. REAL and J. R. VILCHE, in *Transient Techniques in Corrosion Science and Technology* (eds W. H. SMYRL, D. D. MACDONALD and W. J. LORENZ), pp. 88–100. The Electrochemical Society Inc., Pennington (1989).
27. I. OLEFJORD and B. BROX, in *Passivity of Metals and Semiconductors* (ed. M. FROMENT), pp. 561–570. Elsevier, Amsterdam (1983).
28. V. JOVANCICEVIC, R. KAINTHLA, Z. TANG, B. YANG and J. O'M. BOCKRIS, in *Surfaces, Inhibition and Passivation* (eds E. MCCAFFERTY and R. Y. BRODD), pp. 192–209. The Electrochemical Society Inc., Pennington (1986).
29. J. O'M. BOCKRIS, *Corros. Sci.* **29**, 291 (1989).
30. YU. V. PLESKOV and V. YU. FILINOVSKII, *The Rotating Disc Electrode*. Consultants Bureau, New York (1976).
31. V. G. LEVICH, *Physicochemical Hydrodynamics*. Prentice Hall, Englewood Cliffs, New Jersey (1962).
32. M. POURBAIX, *Atlas of Electrochemical Equilibria*, p. 307. Pergamon Press, Oxford (1966).
33. P. G. SINGER and W. STUMM, *J. AWWA Am. Conf.*, p. 196 (1968).
34. T. A. CARLSON, *Photoelectron and Auger Spectroscopy*. Plenum Press, New York (1975)
35. D. BRIGGS and M. P. SEAH (eds), *Practical Surface Analysis by Auger and X-Ray Photoelectron Spectroscopy*. Wiley, London (1983).
36. D. H. DAVIES and G. T. BURSTEIN, *Corrosion* **36**, 416 (1980).
37. J. G. N. THOMAS, T. J. NURSE and R. WALKER, *Br. Corros. J.* **5**, 87 (1970).
38. M. COHEN and K. HASHIMOTO, *J. Electrochem. Soc.* **121**, 42 (1974).
39. A. M. RILEY and J. M. SYKES, in *Passivity of Metals and Semiconductors* (ed. M. FROMENT), pp. 661. Elsevier, Amsterdam (1983).
40. R. D. ARMSTRONG and A. C. COATES, *J. electroanal. Chem.* **50**, 303 (1974).
41. P. SOUTHWORTH, A. HAMNETT, A. M. RILEY and J. M. SYKES, *Corros. Sci.* **18**, 1130 (1988).